J Neurophysiol 107: 836–849, 2012.
First published November 9, 2011; doi:10.1152/jn.00063.2011.

Spiking and LFP activity in PRR during symbolically instructed reaches

Eun Jung Hwang and Richard A. Andersen
Division of Biology, California Institute of Technology, Pasadena, California

Submitted 24 January 2011; accepted in final form 8 November 2011

Hwang EJ, Andersen RA. Spiking and LFP activity in PRR during symbolically instructed reaches. *J Neurophysiol* 107: 836–849, 2012. First published November 9, 2011; doi:10.1152/jn.00063.2011.—The spiking activity in the parietal reach region (PRR) represents the spatial goal of an impending reach when the reach is directed toward or away from a visual object. The local field potentials (LFPs) in this region also represent the reach goal when the reach is directed to a visual object. Thus PRR is a candidate area for reading out a patient's intended reach goals for neural prosthetic applications. For natural behaviors, reach goals are not always based on the location of a visual object, e.g., playing the piano following sheet music or moving following verbal directions. So far it has not been directly tested whether and how PRR represents reach goals in such cognitive, nonlocational conditions, and knowing the encoding properties in various task conditions would help in designing a reach goal decoder for prosthetic applications. To address this issue, we examined the macaque PRR under two reach conditions: reach goal determined by the stimulus location (direct) or shape (symbolic). For the same goal, the spiking activity near reach onset was indistinguishable between the two tasks, and thus a reach goal decoder trained with spiking activity in one task performed perfectly in the other. In contrast, the LFP activity at 20–40 Hz showed small but significantly enhanced reach goal tuning in the symbolic task, but its spatial preference remained the same. Consequently, a decoder trained with LFP activity performed worse in the other task than in the same task. These results suggest that LFP decoders in PRR should take into account the task context (e.g., locational vs. nonlocational) to be accurate, while spike decoders can robustly provide reach goal information regardless of the task context in various prosthetic applications.

sensory-motor; visuomotor and motor neurons; parietal cortex; symbolic reach; direct reach; neural prosthetics

IN VISUALLY GUIDED REACHING, the spatial goal of the reach can have various relationships to a visual object (Wise et al. 1996). Since no conventionally accepted nomenclature exists for these different relationships, we will use the following definitions throughout the paper. In the direct reach, the visual object is the reach goal. In the transformational reach, the goal is inverted, rotated, or scaled from the visual object location. In both direct and transformational reaches, the spatial location of the object is used to compute the reach goal. In the symbolic reach, the goal is associated with nonlocational features such as shape or color. The shape or color of the stimulus holds no intrinsic relation to the reach goal but can be reliably associated with a specific reach goal after training.

In the parietal reach region (PRR) of posterior parietal cortex, neurons systemically vary their firing rate with the impending reach goal for both direct and transformational reaches (Gail and Andersen 2006; Snyder et al. 1997). However, it has not been directly investigated whether and how spiking activity in PRR encodes the reach goal for symbolic reaches in which the goal is inferred from nonlocational features of an object. It seems reasonable to expect that the spiking activity in PRR would encode the goal for a symbolic reach considering that it encodes the goal in the antireach task, a transformational reach in which the goal is inverted from the stimulus location (Gail and Andersen 2006; Gail et al. 2009; Westendorff et al. 2010). Moreover, for the same reach goal, the response of a majority of neurons in the antireach task was similar to the proreach task, a direct reach, and the response of only ~20% of neurons was gain-modulated by the task condition (Gail et al. 2009). The spiking activity of PRR for symbolic reaches may not significantly differ from direct reaches similar to the spiking activity of PRR for transformational reaches.

Increasingly more studies in neural prosthetic research pay attention to the encoding properties of local field potentials (LFPs), as LFPs are less sensitive to changes in the electrode position than spike waveforms, and thus possibly more stable in a chronic recording situation (Andersen et al. 2004; O'Leary and Hatsopoulos 2006). So far the reach goal encoding of LFPs in PRR has been examined only in direct reach tasks. LFPs in PRR modulate their spectral power in high beta and low gamma bands depending on the location of the goal for impending direct reaches in PRR (Hwang and Andersen 2011; Scherberger et al. 2005). In our previous study in PRR, we showed that the gamma band LFPs at above 40 Hz encode the reach goal more strongly when the stimulus at the goal remains visible than when the stimulus is extinguished and the monkey has to remember the stimulus location (Hwang and Andersen 2011). Therefore, the LFPs in PRR appear to encode the goal in a task-specific manner. It is of interest to find whether and which components of the LFPs differ between symbolic and direct reaches.

Examination of the goal encoding properties of spikes and LFPs recorded from PRR in various reach tasks will provide important information regarding how to build decoders that perform robustly across various neural prosthetic applications (Andersen and Cui 2009; Andersen et al. 2010). If the neural activity in PRR represents the reach goal for symbolically cued reaches, this region could provide control signals for a neural prosthesis even when the goal is designated in this more cognitive way. Furthermore, if the population response in symbolic tasks is identical to that in direct tasks, then a single algorithm trained in a simple calibration task could be used to decode the intended reach goal for a variety of conditions.

To address these issues, we examined the spiking and LFP activity of the macaque PRR with a symbolic reach task and compared this activity to responses recorded with a direct reach task. We found that the spiking activity near reach onset represents the reach goal in a task-invariant manner, allowing

Address for reprint requests and other correspondence: E. J. Hwang, Div. of Biology, Mail Code 216-76, California Inst. of Technology, Pasadena, CA 91125 (e-mail: eunjung@caltech.edu).

perfect decoding of the reach goal with a single decoder across task conditions. The LFP activity at 20–40 Hz showed a small but significantly enhanced goal representation in the symbolic task, resulting in a decrease in decoding accuracy when applying the decoder to the direct reach task. Therefore, decoders using LFP activity should take into account the task condition, while decoders using PRR spiking activity can robustly provide reach goal information without considering the task condition.

METHODS

Two male rhesus monkeys (*Macaca mulatta*; *monkey Y*: 7 yr, *monkey G*: 6 yr) participated in this study. All procedures were in accordance with National Institutes of Health guidelines and were approved by the California Institute of Technology Animal Care and Use Committee.

Behavioral tasks: direct versus symbolic task. The monkeys sat in a primate chair and viewed visual stimuli presented on a vertical LCD monitor placed in the fronto-parallel plane, ~40 cm away from the eyes. The monkeys' eye position was recorded with an infrared CCD camera (240 Hz; ISCAN, Burlington, MA), and hand position was recorded with a 19-in. translucent touch-sensitive screen (IntelliTouch; ELO Systems, Menlo Park, CA) placed in front of the LCD monitor. The visual stimulus presentation, online monitoring of eye and hand positions, and reward delivery were controlled by a real-time LabView program (National Instruments, LabView7.1) running on a real-time operating system (National Instruments, LabView RealTime).

The direct task trials began with the monkeys acquiring the ocular and manual fixations in the center of the screen (Fig. 1*A*). After a 0.5-s fixation period, a single reach target (circle) was flashed for 0.3 s at one of six peripheral locations evenly spaced around a virtual circle (radius ~10.3° eccentricity). The monkeys maintained fixation for a variable delay (random between 1.2 s and 1.5 s) until the manual fixation target disappeared (go-cue), signaling them to reach to the remembered location without moving the eyes. After holding the hand within 3° from the reach target and the eyes on the fixation target for 0.3 s, they received a juice reward.

The symbolic task trials proceeded in the same way as the direct task trials except that an arrow at the central fixation location instead of a circle in the periphery was presented during the cue period (Fig. 1*B*). The correct reach target was in the pointing direction of the arrow on the same virtual circle as in the direct task. The monkeys learned the imposed rules over a course of 3–4 wks, and during the recording experiment they performed with high accuracy (95 ± 8.0% for *monkey Y*, 84 ± 14.7% for *monkey G*). The task types and target locations were pseudorandomly interleaved. Twelve trials per target location and trial type were included in the analysis of each neuron or LFP site.

The reaction time from the go-cue to reach onset was 273 ± 98.1 ms and 267 ± 86.4 ms, respectively, in the direct and symbolic tasks for *monkey Y* and 433 ± 170.0 ms and 431 ± 191.3 ms for *monkey G*.

Extracellular recording. Both monkeys were implanted with a head holder and recording chamber over the intraparietal sulcus following the procedures described by Scherberger et al. (2003). A 16-channel chronic microdrive (Neuralynx, Bozeman, MT) was housed in the chamber and removed at the end of the study. The recording chamber placement was guided and confirmed by structural magnetic resonance imaging.

We recorded 229 neurons in total (104 from *monkey Y*, 125 from *monkey G*) from the cortical region within which a majority of neurons show stronger direct reach delay period activity than direct saccade delay period activity. The recording area was confined to 0–5 mm posterior and 5.5–8 mm lateral in Horsley-Clarke coordinates, at

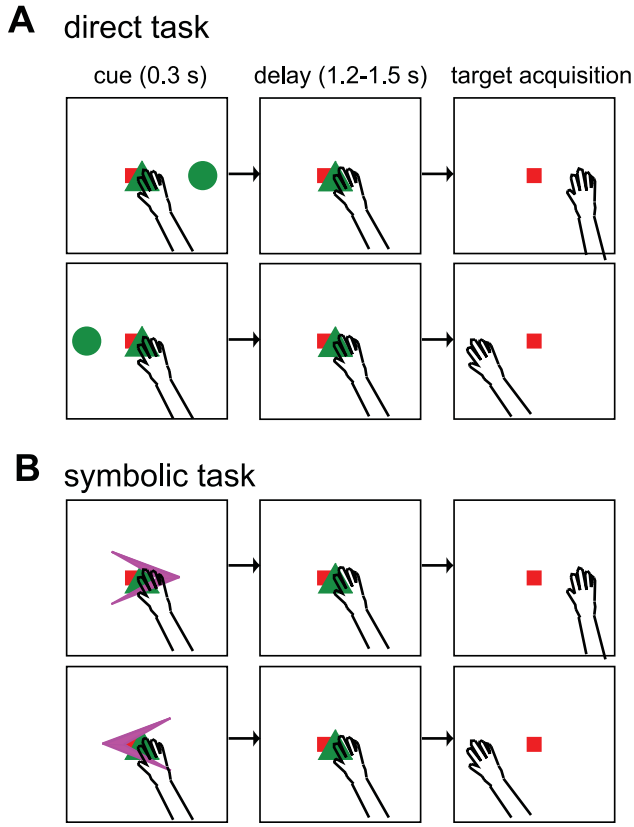

Fig. 1. The 2 randomly interleaved tasks. *A*: direct task. Monkeys reached to the remembered location of a briefly flashed visual stimulus (green circle). The monkey's gaze was fixed on the center of the monitor (red square) throughout the trial. *B*: symbolic task. To be rewarded, monkeys reached in the direction of a briefly flashed arrow in the central visual field after the imposed variable delay. Note that icons are not to scale.

3–7 mm below the dural surface, for *monkey Y* and ~6–10 mm posterior and 6.5–10 mm lateral, at 3–7 mm below the dural surface, for *monkey G*. Of the 229 neurons, we included in our analyses only the neurons that satisfied the following two criteria: *1*) its delay period (1-s interval prior to reach onset) activity was significantly tuned to the reach goal in at least one of the two reach tasks (1-way ANOVA with the reach goal as the single factor, $P < 0.01$), and *2*) the maximum mean firing rate during the delay period exceeded 5 Hz. In total 178 neurons recorded from 159 recording sites qualified these criteria (85 neurons from *monkey Y*, 93 from *monkey G*).

The LFP signals were separated from the spiking signals by a preamplifier (Plexon MAP system) with built-in hardware band-pass filters (LFP: 3.3–88 Hz, spike: 154 Hz-8.8 kHz). The cutoff frequencies of the LFP filters were predetermined based on previous findings in our laboratory that the cognitive state or reach goal information encoded in LFPs during the delay period is concentrated below ~90 Hz (Hwang and Andersen 2009; Pesaran et al. 2002; Scherberger et al. 2005).

Spatial tuning analysis. Hereafter, the late delay period is the 1-s time interval prior to the go-cue unless otherwise noted. The spike and LFP signals in the late delay period were subjected to spatial tuning analysis. For the spike signal, the spike count in the late delay period was used. For the LFP signal, the spectral power in the late delay period was computed by the multitaper method with a 5-Hz bandwidth (Pesaran et al. 2002), and the average powers in eight frequency bands (0–10, 10–20, . . . , 70–80 Hz) were analyzed. The spatial tuning properties of both the spike and LFP signals were analyzed in terms of tuning depth, circular variance, and preferred direction as described below.

Tuning depth and circular variance. The tuning depth was computed as the trough-to-peak amplitude of a tuning curve that characterized the mean signal variation as a function of the reach goal. The tuning depth for the spike signal was computed on spike counts. The tuning depth for the LFP signal was computed on the LFP spectral power converted into the percent change from the baseline (0.2-s interval before cue onset) spectrum.

On the other hand, the width of the tuning curve was computed using circular variance as follows (Gur et al. 2005):

$$1 - \left| \sum_{i=1}^{6} \left(r_i \cdot \vec{u_i} \right) / \sum_{i=1}^{6} r_i \right|$$

Here r_i is the mean signal value for the ith target location and

$$\vec{u_i}$$

is the unit vector pointing to the ith target. The six target locations differed only in their direction but not in eccentricity. The circular variance varies between 0 and 1; the lower the circular variance, the sharper the tuning.

The statistical significance of both the tuning depth and the circular variance of each tuning curve was tested through a permutation test. The trial-by-trial data were randomly permuted so that each trial was assigned with a random target location but with the same task condition as the original data, and the tuning depth and circular variance of the permuted sample were computed. After 1,000 repetitions, if the 99% confidence interval of the 1,000 permuted samples did not include the unpermuted data, we considered that the tuning depth or circular variance was significant at the 1% significance level.

Preferred direction. The preferred direction was determined as the directional tuning vector (DTV) computed as follows:

$$\mathrm{DTV} = \sum_{i=1}^{6} r_i \cdot \vec{u_i}$$

(Gail and Andersen 2006). Given the noise in the signals and the limited number of trials, six targets may not be sufficient to accurately estimate the preferred direction. However, the DTV-based preferred direction has been used for as few as four targets (Gail and Andersen 2006). Moreover, we took steps to reduce the false alarm errors in determining whether two preferred direction estimates from the DTV-based method were different through a bootstrapping method described in the next section.

Statistical significance test for intertask difference. We applied a bootstrapping method proposed by Stevenson et al. (2011) to determine the statistical significance of the intertask difference for each variable (tuning depth, circular variance, mean firing rate, and preferred direction) at the individual neuron and LFP site level. We computed the confidence interval of the intertask difference through 1,000 time bootstrap resamplings of trials. Each time, we randomly sampled 72 trials with replacement from the original data for each of the two tasks and computed the intertask difference in the variable of interest from the sample. After 1,000 repetitions, if the 99% confidence interval of the intertask difference did not contain 0, then we rejected the null hypothesis (that the difference actually is 0) at the 1% significance level.

To determine the statistical significance of the intertask difference at the population level, we applied the *t*-test on the population sample of the difference for the tuning depth and mean firing rate. For the circular variance, we applied the Wilcoxon signed-rank test because the difference in the circular variance is a bounded variable. For the preferred direction, we applied the circular m-test, which is equivalent to the linear *t*-test.

For any statistical tests on the preferred direction except for the permutation test described above, we used the Matlab Circular Statistics Toolbox provided by Berens.

Peristimulus time histogram. When estimating the time when the firing rates are significantly tuned to the reach goal, we wanted to use spiking events that occurred up to that time and not after. Therefore, instead of the conventional Gaussian kernel method, we applied the procedures described in Westendorff et al. (2010) to construct the peristimulus time histogram (PSTH). The raw spike train with 1-ms resolution was aligned to cue onset or reach onset and convolved with the following excitatory postsynaptic potential (EPSP)-like causal kernel:

$$\frac{0.022}{0.02^2} \cdot \left(1 - e^{\frac{-t}{0.002}}\right) \cdot e^{\frac{-t}{0.02}} \cdot w(t)$$

where

$$w(t) = \begin{cases} 1, & \text{if } t \geq 0 \\ 0, & \text{otherwise} \end{cases}$$

Then, it was convolved with a causal 20-ms-long rectangular kernel:

$$\begin{cases} 1, & \text{if } 0 \leq t < 0.02 \\ 0, & \text{otherwise} \end{cases}$$

The causal kernel resembling a postsynaptic potential in combination with the rectangular kernel represents the smoothed postsynaptic influence of each spike (Thompson et al. 1996).

Reach goal tuning latency. We computed reach goal tuning latency of individual neurons as described by Westendorff et al. (2010). For an individual neuron, the PSTH values at each time point (with 1-ms steps) were subjected to a one-way ANOVA test with the reach goal as the single factor and to the DTV computation. The reach goal tuning at a specific time point was considered to be significant if the ANOVA test was significant at $P < 0.05$ and the amplitude of the DTV was greater than 20% of the value for the maximally responding reach goal at that time point. When the reach goal tuning was significant for a consecutive 50-ms duration for the first time after cue onset, the initial time point of the 50-ms duration was taken as the reach goal tuning latency.

Classification of neurons. Previously, we defined two PRR neuron classes, visuomotor and motor (Hwang and Andersen 2011). The classification used the following definitions. When planning a reach to the preferred goal, the visuomotor neurons fire more when the goal stays illuminated (visual task, similar to the direct task in this study but the visual stimulus at the goal stayed illuminated until the end of the trial) than when it is extinguished (memory task, same as the direct task in this study). In contrast, the motor neurons fire at the same rate whether or not the goal stays illuminated. Since some neurons ($N = 129$) in this study were recorded during the visual task as well, we could classify these neurons as visuomotor and motor based on their response difference between the visual and memory tasks in the same way as the previous study. That is, we classified a neuron as visuomotor if its delay period response from 1.2 to 0.2 s before reach onset was greater in the visual than memory task by at least 3 spikes/s, and as motor otherwise.

LFP spectrogram. The raw LFP trace from each trial was transformed to a power spectrogram by computing a sequence of spectra over the 200-ms windows sliding with 50-ms steps, using the multitaper method with a 10-Hz bandwidth (Pesaran et al. 2002). Note that the bandwidth in the temporal analysis was larger than the spatial tuning analysis because of the smaller temporal window. The baseline power for each frequency was computed from the mean spectrum in the baseline period, averaged across all trials. The baseline period was a 200-ms interval preceding cue onset. The spectrogram of each trial was normalized to the percent change from the baseline spectrum. That is, the change from the baseline power was divided by the baseline power.

Reach goal decoding. To assess the feasibility of a single decoder in varying task conditions, we trained a Bayesian maximum likelihood

classifier using data in one task and tested its performance in the other task (Salinas and Abbott 1994).

For each neural signal observation, we selected the target that was the most likely to be associated with the observation as follows. For a given observation, x, we computed the probability of each target conditional on the given observation, i.e., the posterior probability, $P(\text{target}_i \mid x)$, and selected the target with the maximum posterior probability: $\overset{\text{argmax}}{i} P(\text{target}_i \mid x)$ as the decoder output. The posterior probability was computed following Bayes' rule using the prior and the probability of the observation conditional on each target location:

$$P(\text{target}_i \mid x) = P(x \mid \text{target}_i) \cdot P(\text{target}_i) / P(x)$$

Since we assumed that the prior, $P(\text{target}_i)$, was uniform among the targets and $P(x)$ was common among the targets, the target that maximizes $P(\text{target}_i \mid x)$ must maximize $P(x \mid \text{target}_i)$.

In addition, we assumed that $P(x \mid \text{target}_i)$ was normally distributed, the variance, σ^2, was common, and only the mean, m_i, was different among the targets. Therefore, $P(x \mid \text{target}_i)$ was maximal when the exponent of the normal function, $-(x - m_i)^2/2\sigma^2$, was maximal. For a given x, the exponent is maximal when $(2x \cdot m_i - m_i^2)/2\sigma^2$ is maximal. Thus the decoder needed to compute only this linear formula for each observation using m_i and σ^2 estimated from the training data to determine the most probable target.

For a N-dimensional observation signal (e.g., spike counts of N neurons), the linear formula can be rewritten in a matrix form as follows:

$$\overset{\text{argmax}}{i} x^T v^{-1} M_i - 0.5 \cdot M_i^T v^{-1} M_i, \left(1 \le i \le 6\right)$$

Here, v is a $N \times N$ diagonal matrix with the variance of each dimension of the observation signal in the diagonal, and M_i is a $N \times 1$ vector with the mean for the ith goal. The variance matrix was diagonal, as we assumed that different elements of observation signals were independent from one another. In the decoding analysis, we used spike counts and/or log powers in the eight frequency bands for LFP signals.

To examine the time course of decoding performance, a decoder was applied to the spike count or log power in 200-ms sliding windows with 50-ms steps starting from cue onset. In each time step, we used the observation signal that occurred only up to that time point and not after. The time course was computed in two different ways. In the first analysis, for each time point, training data were sampled from that time point. This analysis informed us how soon after cue onset reach goal information could be reliably extracted.

In the second analysis, training data were sampled from a constant time point. The idea is that in brain-machine interface (BMI) applications, the decoder would not be able to appropriately apply time-selective training data because there is no event defined as cue onset. Thus it is more realistic to use a constrained training data set across time points. Since the neural response immediately before reach onset is known to be less variable across trials and across task conditions (Churchland et al. 2010; Crammond and Kalaska 2000), training data for the second analysis were sampled from the time window immediately before reach onset. An important question is whether it is realistic to use movement onset in a real prosthetic application. In a previous study, we showed that monkeys can be trained to emit a specific LFP signal to move a computer cursor at an intended movement onset time without moving their own limbs (Hwang and Andersen 2009). Therefore the intended movement onset time can be read out from the brain, and the spikes or LFPs that occurred just prior to that time can be used to decode the intended goal of the movement.

In addition, we examined the effect of time window length on the decoding performance by varying the length from 200 to 1,200 ms.

The decoder was tested in all 72 trials (12 trials/goal $\times$ 6 goals), one at a time. The decoding performance was defined as the proportion of correctly decoded trials. Leave-one-out cross-validation was used when training data were from the same task. When testing decoding across tasks, to match the number of training data points to the within-task decoding, for each trial in one task 71 trials were randomly selected from the other task as training data. To simulate a large population recording, we concatenated sequentially recorded spiking and LFP signals as if they were simultaneously recorded. However, it is noteworthy that our decoding algorithm assumes independence between the different channels and is likely to produce poorer decoding performance when used for simultaneously recorded multichannel neural signals, especially in the case of LFPs, because of correlations between the recorded signals.

RESULTS

Spiking activity in late delay period is task-invariant. To address whether and how PRR represents a reach goal derived symbolically in comparison to a reach goal directed to a visual stimulus, we compared the spiking and LFP activity between the symbolic and direct tasks (Fig. 1). Figure 2 shows the spiking activity of two typical PRR neurons, *neurons A* and *B*, when the monkey reached to the preferred or antipreferred goals in both tasks. In the direct task, *neuron A* increased its firing rate with a strong transient response upon cue onset and maintained a high level of activity until reach onset if the impending reach was to the preferred direction (Fig. 2*A*). In the symbolic task, it lacked the transient response yet increased its firing rate for the preferred goal so that the sustained activity during the later delay period became nearly identical to that in the direct task (Fig. 2*B*). The spiking activity for the antipreferred goal was similarly low in both tasks. Accordingly, the spatial tuning of *neuron A* during the late delay period (1-s period prior to the go-cue) was similar between the two tasks with matching spatial preference and tuning strength (Fig. 2*C*). Unlike *neuron A*, *neuron B* lacked a strong transient response in the direct task for the preferred goal. However, it increased its firing rate to sustain a high level of activity selectively for the preferred goal in both tasks, and the spatial tuning of the late delay period response was indistinguishable between the two tasks, similar to *neuron A*.

In a previous study, we defined two PRR neuron classes, visuomotor and motor, based on their sensitivity to visual stimulation of the reach target during the delay period from 1.2 to 0.2 s before reach onset (Hwang and Andersen 2011). The visuomotor neurons, like *neuron A*, have strong transient responses upon cue onset in their preferred goal location, but the motor neurons, like *neuron B*, do not. Since many neurons ($N = 129$) in this study were recorded during the previous study as well, we could classify these neurons as visuomotor and motor (see METHODS) and examine the intertask difference separately for the two classes. Of 129 neurons (80 from *monkey Y*, 49 from *monkey G*), 40 neurons (29/80, 11/49; 31%) were visuomotor and the rest (51/80, 38/49; 69%) were motor. In the direct task, the visuomotor neurons showed a transient response to cue onset (Fig. 3*A*). Not surprisingly, the visuomotor neurons showed reach goal tuning earlier than the motor neurons in the direct task (Fig. 3*C*). The distribution of the reach goal tuning latency was significantly different between the two classes (2-sample Kolmogorov-Smirnov test, $P < 0.01$). In the symbolic task, both classes of neurons increased their firing rate for the preferred goal at similar rates and without transients (Fig. 3*C*). The reach goal tuning latency

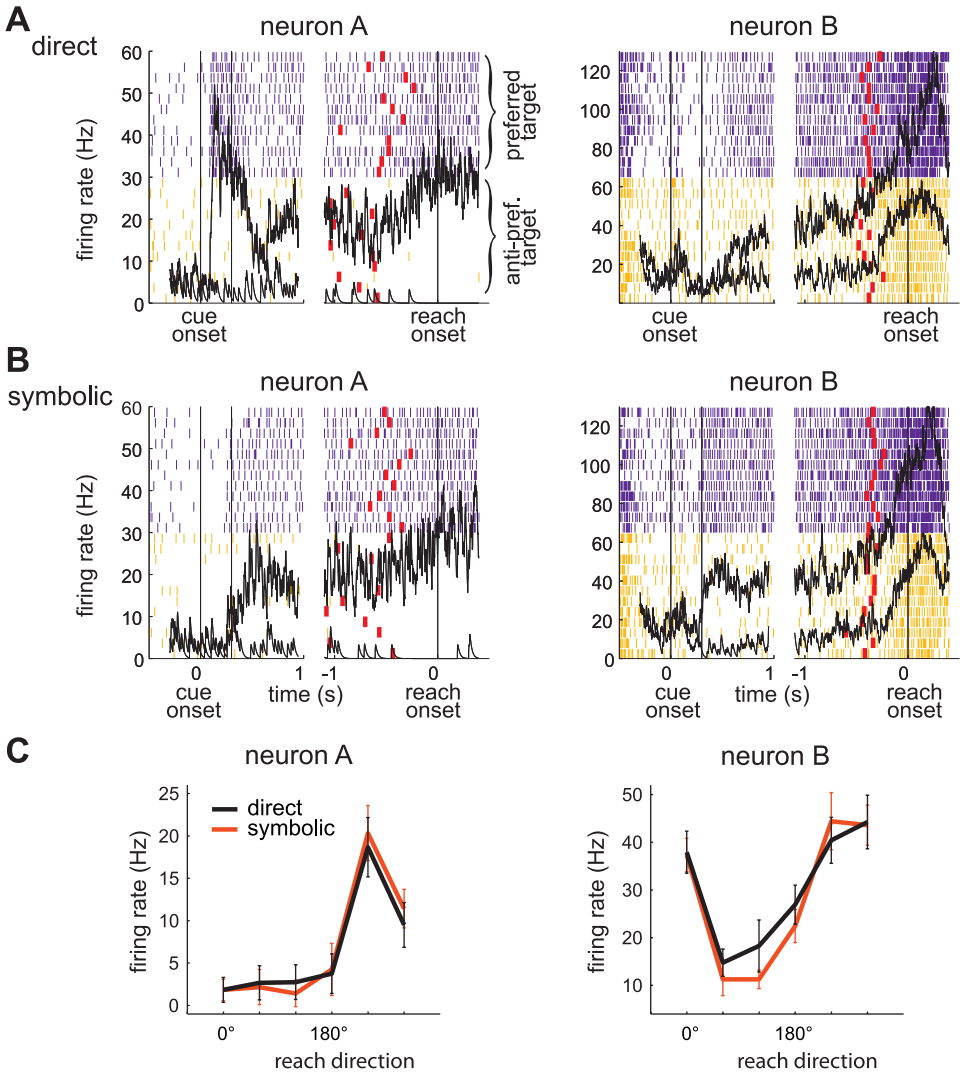

Fig. 2. Spiking activity of 2 example parietal reach region (PRR) neurons. *A*: spike rasters when the preferred target (purple) or anti-preferred target (orange) is the reach goal in the direct task. Mean peristimulus time histograms (PSTHs; black lines) are superimposed. Spike rasters and PSTHs are broken into 2 parts with the left side aligned to cue onset and the right side aligned to reach onset. Red ticks mark the go-cue. *B*: spike rasters and mean PSTHs in the symbolic task for the same neurons shown in *A*. *C*: mean (±SD) firing rate during the late delay period (1-s period prior to reach onset) for each of 6 reach directions (0° being to the right and measured counterclockwise) of the same neurons in *A* and *B*.

distribution was not significantly different between the two classes for the symbolic task (2-sample Kolmogorov-Smirnov test, $P > 0.01$).

Despite the difference in early period response between the two classes, both classes showed task-invariant spatial tuning in the late delay period (Fig. 3, *A* and *B*). Thus, for the late delay period response, we present the analysis results using all neurons that were recorded in the direct and symbolic tasks ($N = 178$; 85 from *monkey Y*, 93 from *monkey G*) without distinguishing their class. We first examined the significance of the reach goal tuning in the late delay period based on a one-way ANOVA with the reach target as the single factor, at the significance level of $P < 0.01$. We found that 79% of neurons (78/85 for *monkey Y*, 63/93 for *monkey G*) were significantly tuned in the late delay period in both tasks, 10% (7/85, 11/93) only in the symbolic task, and 8% (0/85, 14/93) only in the direct task.

We further examined the difference in the reach goal tuning between the two tasks in terms of the preferred direction, tuning depth, circular variance, and mean firing rate at both the population and individual neuron levels (summarized in Table 1).

First, the preferred direction was not different between the two tasks at the population level (circular m-test; $P > 0.01$) (Fig. 4, *A* and *B*). Figure 4*A* shows the preferred direction in the direct task versus the symbolic task of all 178 neurons. The majority of neurons lie close to the unity line, indicating that the preferred direction was similar between the two tasks. At the individual neuron level, we found that the preferred direction was not statistically different between the tasks for 89% of neurons (bootstrap, $P > 0.01$; 71/85, 88/93). The high incidence of nearly identical preferred directions between the two tasks cannot be explained by any intrinsically biased representation of preferred directions because the null distribution (distribution of differences in preferred direction for randomly paired neurons) is rather uniform (Fig. 4*B*).

Second, we compared the tuning depth (maximum firing rate − minimum firing rate in the tuning curve) between the two tasks because the amplitude of the tuning curves could be different even with similar preferred directions (Fig. 4, *C* and *D*). The tuning depth was statistically significant for 84% of the neurons (77/85, 73/93) in the direct task and 87% (83/85, 72/93) in the symbolic task (permutation test, $P < 0.01$). Tuning depth was not significantly different between the two tasks at the population level (*t*-test; $P > 0.01$). At the individual neuron level, the tuning depth was

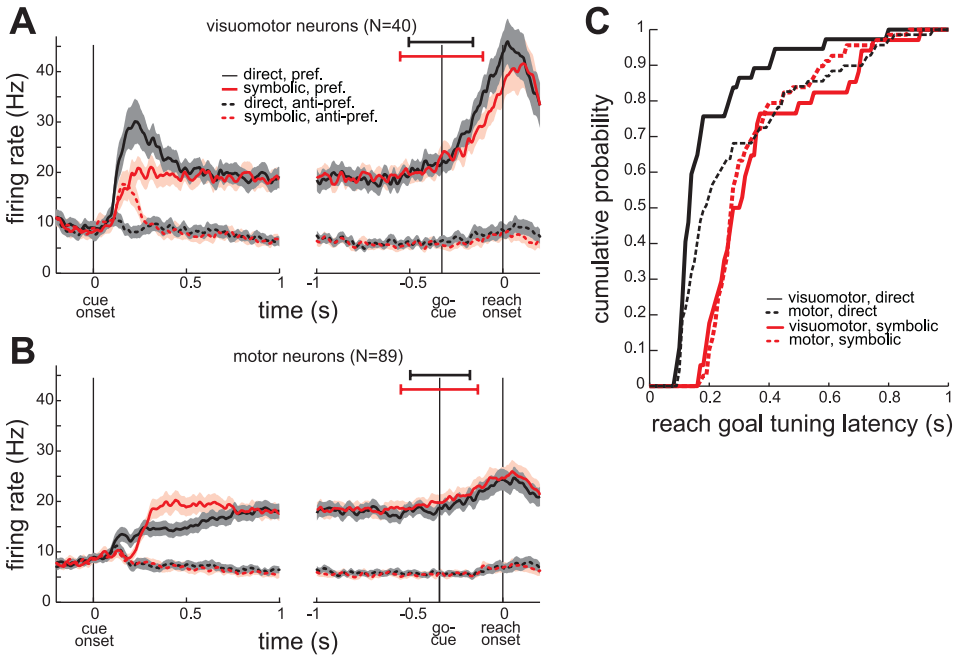

Fig. 3. Average time courses of firing rate of 2 neuronal classes. *A*: average PSTHs (mean ± SE) of visuomotor neurons ($N = 40$), aligned to cue onset and reach onset. Horizontal bars superimposed on the go-cue indicate ±SD of the go-cue relative to reach onset in the direct (black) and symbolic (red) tasks. *B*: same as *A* but for motor neurons ($N = 89$). *C*: cumulative probability of the tuning response latency separately for each neuronal class and task.

not statistically different between the tasks for 77% of the neurons (bootstrap, $P > 0.01$; 71/85, 88/93).

Third, we compared the circular variance representing the width of the tuning curve (Fig. 4, *E* and *F*). The circular variance was statistically significant for 83% of the neurons (76/85, 71/93) in the direct task and 84% (82/85, 68/93) in the symbolic task (permutation test, $P < 0.01$). We found no difference between the two tasks at the population level (Wilcoxon signed-rank test; $P > 0.01$). At the individual neuron level, the circular variance was not statistically different between the tasks for 86% of the neurons (bootstrap, $P > 0.01$; 55/85, 80/93).

Finally, we examined the possibility of a difference in mean firing rate between the two tasks (Fig. 4, *G* and *H*). The mean firing rate may increase or decrease through a task-modulated gain effect without changing the tuning quality. We found no intertask difference in the mean firing rate at the population level (*t*-test; $P > 0.01$). Individual neuron analysis indicated that the mean firing rate was not statistically different between the tasks for 71% of the neurons (bootstrap, $P > 0.01$; 57/85, 70/93).

Table 1. *Proportion of neurons with significant intertask response difference in terms of tuning depth, circular response, preferred direction, and mean firing*

	% Neurons with Significant Intertask Difference ($P < 0.01$)
Tuning depth	24% (38, 11)
Circular variance	23% (25, 86)
Preferred direction	11% (34, 13)
Mean firing rate	29% (33, 26)

Proportions of neurons with significant intertask response difference in terms of tuning depth, circular response, preferred direction, and mean firing rate ($N = 178$) are shown. Numbers inside parentheses are % for *monkeys Y* and *G*, respectively.

Spatial tuning of LFP activity in the late delay period is enhanced in the symbolic task. Previous studies have shown that LFP power in PRR is modulated by the impending reach goal in the direct task (Hwang and Andersen 2011; Scherberger et al. 2005). However, it remained unknown whether the LFPs still encode the reach goal in nondirect reach tasks such as the transformational or symbolic reach tasks. To address this issue, we examined LFPs in the symbolic task in comparison to the direct task. Figure 5, *A* and *B*, show the power spectrograms of LFPs recorded from the same electrode as *neuron B* in Fig. 2. Consistent with the LFPs reported in the previous studies, the power above 20 Hz of the example LFPs was stronger for the contralateral than the ipsilateral reach goal between cue offset and reach onset in the direct task (Fig. 5*A*). More interestingly, the LFP power above 20 Hz was still modulated in the symbolic task by the reach goal (Fig. 5*B*). The reach goal-related power modulation in both tasks was confirmed in the average power spectrograms across 159 sites from which we recorded single neurons described in the previous section (Fig. 5, *C* and *D*).

To systematically compare the spatial tuning of LFPs between the two tasks, we first examined the tuning depth and circular variance of the late delay period (the 1-s interval prior to the go-cue) LFP power in eight different frequency bands. The tuning depth was significantly larger in the symbolic than the direct task at 30–40 Hz for *monkey Y* and 20–30 Hz for *monkey G* (*t*-test; $P < 0.01$) (Fig. 6*A*). Similarly, the circular variance was significantly smaller in the symbolic than the direct task at 30–40 Hz for *monkey Y* and 20–30 Hz for *monkey G* (Wilcoxon signed-rank test; $P < 0.01$) (Fig. 6*B*). Therefore, the spatial tuning of 20–40 Hz LFPs was enhanced in the symbolic task at the population level. The number of sites that showed significantly different tuning depth or circular variance is listed in Table 2.

Next, we examined the intertask difference in the preferred direction of the late delay period LFPs. In all eight frequency bands, the intertask difference was statistically insignificant at

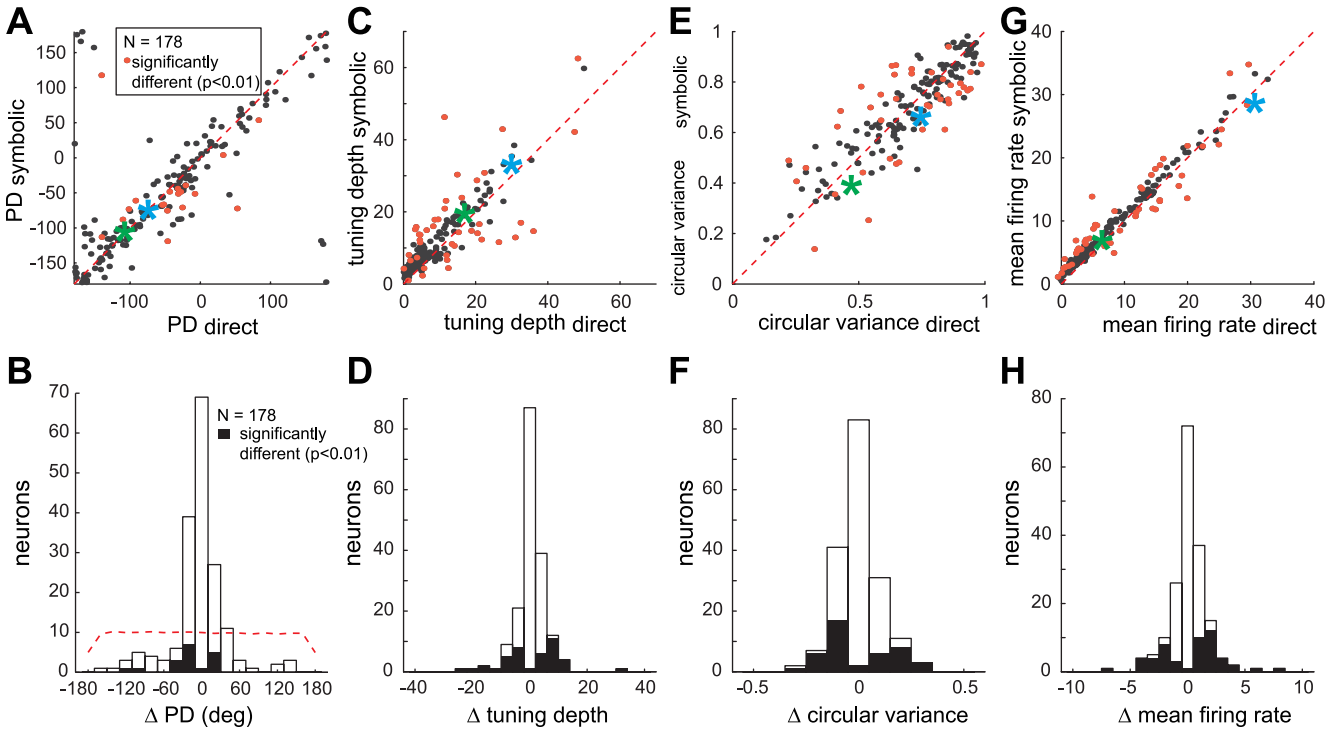

Fig. 4. Spatial tuning of spiking activity during the late delay period. *A*, *C*, *E*, and *G*: comparison between direct and symbolic tasks of the preferred direction (PD), tuning depth, circular variance, and mean firing rates. Each point represents an individual PRR neuron. Red points are neurons with a significant intertask difference ($P < 0.01$). Green asterisk is for *neuron A* in Fig. 1, and blue asterisk is for *neuron B*. *B*, *D*, *F*, and *H*: histogram of difference between the direct and symbolic tasks in preferred direction, tuning depth, circular variance, and mean firing rate. Filled bars represent the number of neurons that show a significant difference between the 2 tasks. Dashed lines in *B* represent the distribution of preferred direction difference for randomly paired neurons.

the population level in both monkeys (circular m-test; $P > 0.01$) and for the majority of the individual LFP sites (Table 2), indicating a consistent spatial preference of the LFPs between the two tasks. The distributions of the intertask differences in the preferred direction confirmed that the preferred directions were nearly identical (Fig. 6, *C* and *D*). For instance, at 20–30 and 30–40 Hz, the peak and the mean of the distributions were located near zero (mean was 7 ± 38.2° and 6 ± 40.8°, respectively). Interestingly, the null distributions (distribution of differences in preferred direction for randomly paired LFP sites) also showed peaks near zero, likely due to the strongly biased spatial preference by the LFPs (Fig. 6, *E* and *F*). Nevertheless, the high incidence of nearly identical preferred directions between the two tasks cannot be explained solely by this intrinsically biased representation because the null distributions were significantly different from the observed distributions (2-sample circular Kuiper test, $P < 0.01$ for both 20–30 and 30–40 Hz bands).

Spike tuning vs. LFP tuning. On average, the tuning quality of spikes was better than that of LFPs. The median circular variance of spikes was 0.73 for both the direct and symbolic tasks. The median circular variance was the smallest in the 0–10 Hz band for LFPs in both tasks and was 0.90 and 0.91 for direct and symbolic tasks, respectively. At the population level, the circular variance was significantly larger for LFPs than for spikes (Wilcoxon signed-rank test, $P < 0.01$ for both tasks). In other words, LFPs were more broadly tuned to the reach goal than spikes.

We wondered whether the tuning quality of spikes could be a good predictor about the tuning quality of LFPs simultaneously recorded from the same electrode. Therefore we computed Pearson's correlation coefficients between the spike and LFP tuning circular variances, and between the spike and LFP tuning depths, across all recording sites. No significant correlation was found in the tuning depth or circular variance between spikes and LFPs in any frequency band or any task. That is, the LFP tuning quality of a given recording site could not be predicted from the spike tuning quality of the same site or vice versa.

We also examined how the preferred directions were related between spikes and LFPs recorded from the same electrode. Figure 7*A* shows the average difference in the preferred directions between spikes and LFPs separately for the eight frequency bands. The preferred direction of the spikes tends to be diametrically opposite from that of the low-frequency band LFPs as indicated by the average difference close to 180°, while it tends to be identical to that of the high-frequency band LFPs as indicated by the average difference close to 0°. To confirm this trend, we computed the correlation coefficient between the tuning curves of spikes and LFPs in the eight frequency bands (Fig. 7*B*). However, the result was inconclusive. The correlation coefficient was positive for the high-frequency bands but not significantly different from zero in the low-frequency bands.

Decoding analysis in the direct and symbolic tasks. First, we asked how quickly after cue onset a decoder trained in one task can reliably predict the reach goal in the same versus the other task. Figure 8*A* shows the average time course of decoding performance when using spiking activity of 178 neurons. In this analysis, for each time window, the decoder was trained by using data from that window only. As predicted by the time course of the firing rates, the reach goal decoding became

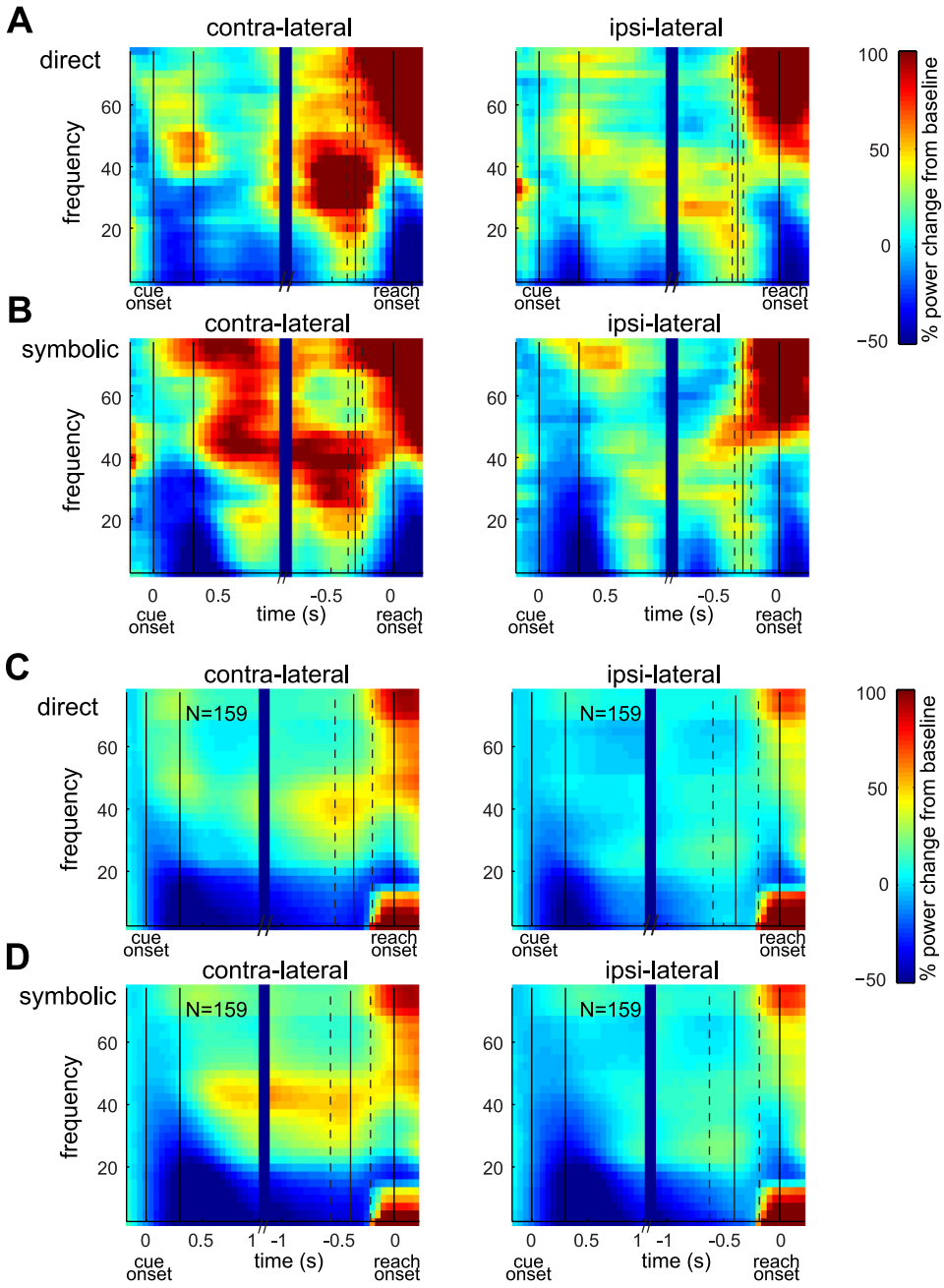

Fig. 5. Local field potential (LFP) power spectrograms. *A*: LFP power spectrogram for a reach target in the space contralateral to the recorded hemisphere vs. ipsilateral side space in the direct task. LFPs were recorded from the same site as *neuron B* in Fig. 2. The left side of the spectrograms is aligned to cue onset, and the right side is aligned to reach onset. Solid vertical lines represent cue onset, cue offset, go-cue, and reach onset. Dashed lines interleaving the go-cue indicate SD. *B*: LFP power spectrograms in the symbolic task for the same recording site as in *A*. *C*: average power spectrograms in the direct task across 159 recording sites. *D*: average power spectrograms in the symbolic task.

accurate earlier in the direct than the symbolic task in both within- and across-task decoding conditions. The decoding performance was significantly better than the chance level (1-sided *t*-test, $P < 0.05$) at 100, 200, 200, and 300 ms, respectively, for direct-direct, symbolic-symbolic, symbolic-direct, and direct-symbolic as training-testing pairs. More interestingly, the across-task decoding performance was not different from the within-task performance at reach onset as both became perfect.

Similar to the spiking activity, when using the LFP activity from 159 sites, the goal decoding became accurate earlier in the direct than the symbolic task (Fig. 8*B*). The decoding performance became significantly better than the chance level at 150, 300, 300, and 300 ms, respectively, for direct-direct, symbolic-symbolic, symbolic-direct, and direct-symbolic as training-testing pairs. Different from the spiking activity, however, the within-task decoding performance stayed significantly better than the across-task performance all the way through reach onset.

A number of factors may contribute to the lower across-task performance when using the LFPs. First, the spatial tuning of the 20–40 Hz LFP power was different between the two tasks in terms of the tuning depth and circular variance as described above. Second, the reliable estimation of LFP power spectra requires longer time windows, especially for lower-frequency power. Thus, as the time window becomes smaller, the relative impact of the 20–40 Hz power on decoding performance would become larger than the lower-frequency power, decreasing the decoding performance in the other task due to the difference in 20–40 Hz power. Consistent with this idea, when we compared the decoding performance at reach onset among various time window lengths used for both training and testing

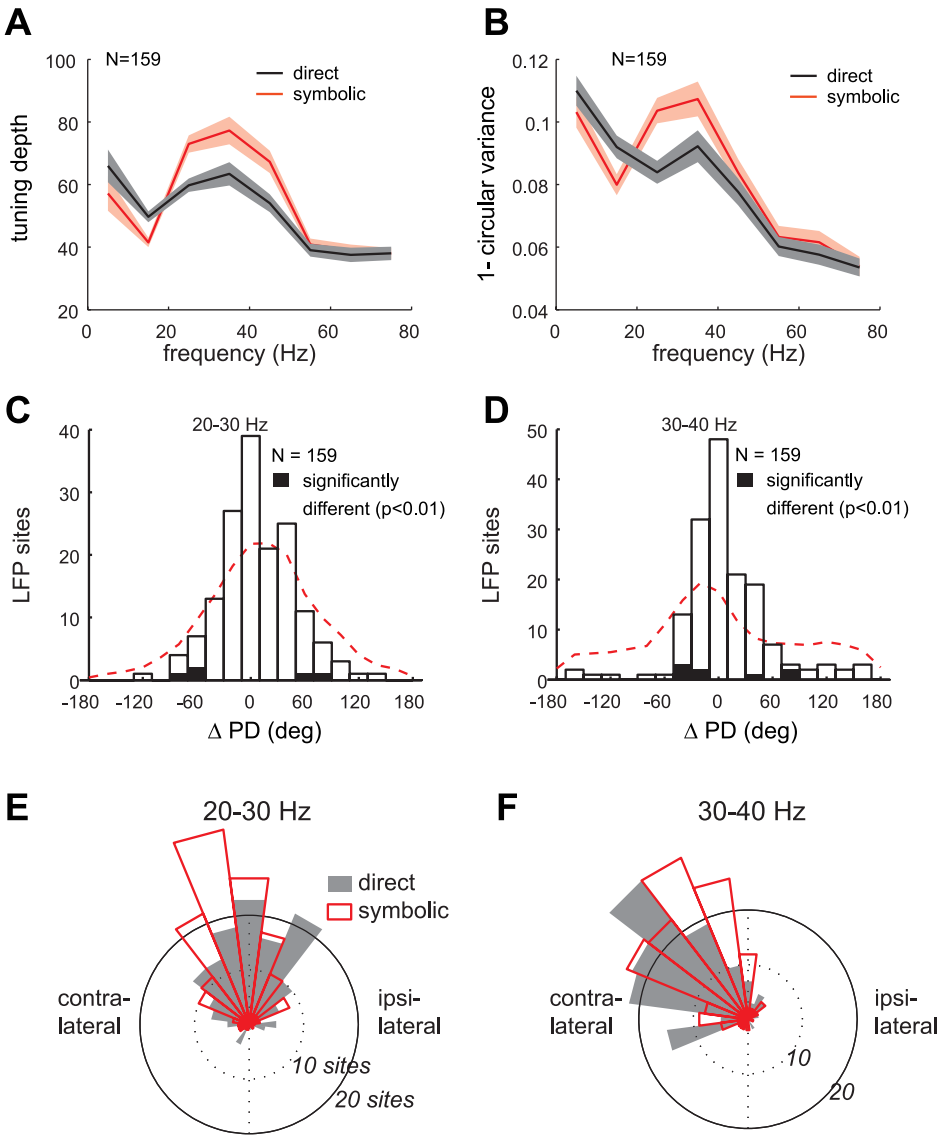

Fig. 6. Spatial tuning of the LFP activity during the late delay period. *A*: average tuning depth of the LFP power (mean ± SE) in the 8 different frequency bands in the direct and symbolic tasks. *B*: average value for (1 − circular variance). *C*: histogram of difference in preferred directions of the 20–30 Hz band power between direct and symbolic tasks. Filled bars represent the number of LFP sites that show significantly different preferred directions between the 2 tasks. Dashed lines represent the distribution of preferred direction differences for randomly paired LFP sites. *D*: same as *C* but for the 30–40 Hz band power. *E*: distribution of the preferred directions of the 20–30 Hz band power in the 2 tasks. *F*: same as *E* but for the 30–40 Hz band.

data, the across-task decoding performance was indeed better with longer window lengths (Fig. 8*C*). However, the difference in the 20–40 Hz power was incompletely compensated for by the use of a more accurate estimate of lower-frequency power using a larger time window. The across-task performance still stayed below the perfect level, reflecting the persistent influence of the difference in the 20–40 Hz power between the two tasks.

Although the analysis heretofore is useful to estimate when one can start accurately predicting the reach goal in laboratory tasks, applying different decoders at different times is not practical for real neural prosthetic applications in which no event defining cue onset exists. Thus it may be more realistic to use a constant training data set across time points. For this purpose, it is sensible to select training data from a time period during which the neural response is the most consistent across and within tasks.

We already showed that the neural response is more consistent between the direct and symbolic tasks near reach onset than earlier time periods. A study of the frontal motor areas reported that the neural response near reach onset is relatively consistent even between an instructed delay task,

Table 2. *Proportion of LFP sites with significant intertask response difference for each of 8 frequency bands in terms of tuning depth, circular variance, and preferred direction*

	0–10 Hz	10–20 Hz	20–30 Hz	30–40 Hz	40–50 Hz	50–60 Hz	60–70 Hz	70–80 Hz
Tuning depth	6% (10, 2)	4% (5, 3)	9% (9, 8)	4% (95, 99)	8% (12, 3)	4% (4, 3)	2% (0, 1)	1% (1, 1)
Circular variance	4% (5, 4)	7% (6, 8)	9% (9, 10)	6% (11, 1)	4% (6, 3)	3% (5, 2)	2% (2, 2)	0% (0, 0)
Preferred direction	4% (5, 4)	4% (6, 3)	3% (1, 5)	4% (5, 3)	1% (0, 3)	1% (1, 1)	0% (0, 0)	1% (1, 0)

Proportions of local field potential (LFP) sites with significant intertask response difference for each of the 8 frequency bands in terms of tuning depth, circular variance, and preferred direction ($P < 0.01$; $N = 159$) are shown. Numbers inside parentheses are % for *monkeys Y* and *G*, respectively.

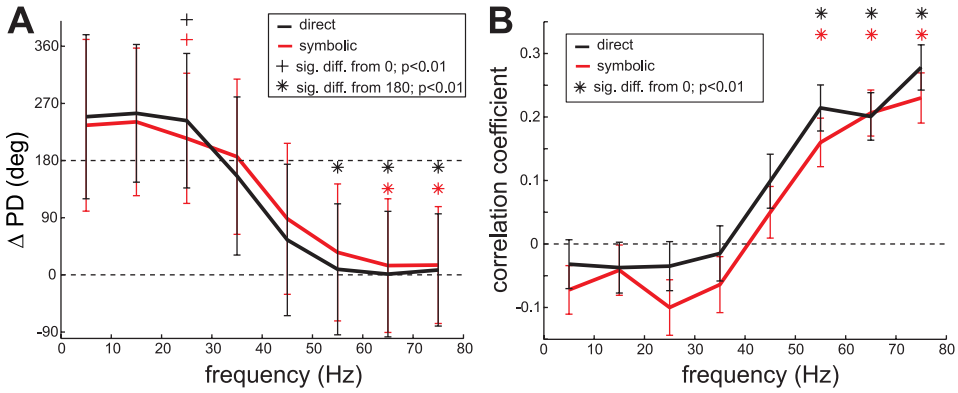

Fig. 7. Relation of the preferred directions between the spiking and LFP activity. *A*: average difference (mean ± SD) between the preferred directions of the spike firing rate and the LFP power in each of the 8 frequency bands. Significance of the difference was tested with the circular m-test. *B*: average correlation coefficient (mean ± SE) between the reach goal tuning curves of the spike firing rate and the LFP power in each frequency band.

like our tasks, and a reaction time task with no instructed delay (Crammond and Kalaska 2000). Furthermore, the population neural response in motor areas is more consistent across trials near reach onset than in other time periods (Churchland et al. 2010). Finally, it is plausible to use movement onset in a real prosthetic application because monkeys can be trained to emit a specific LFP signal to move a computer cursor at an intended movement onset time

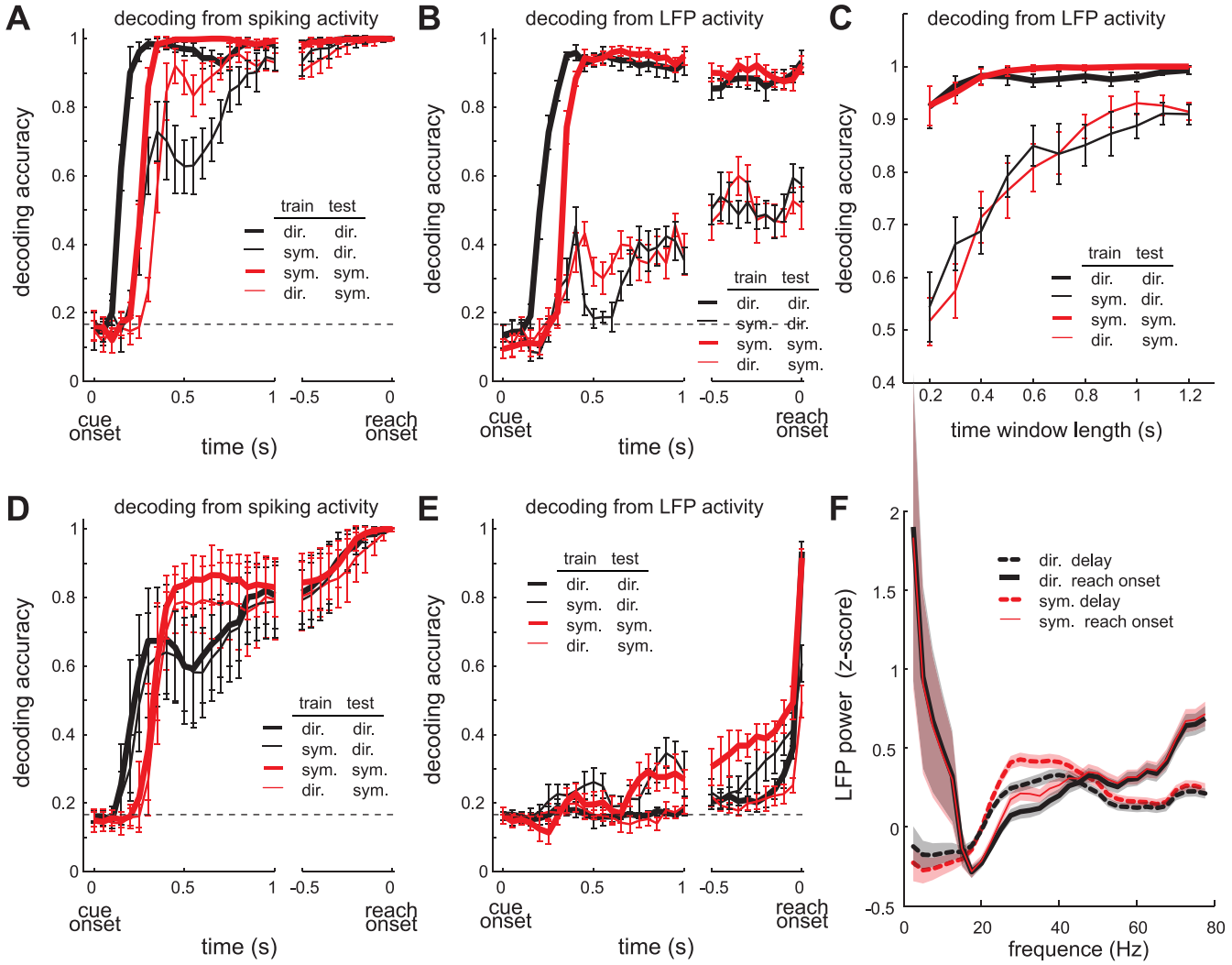

Fig. 8. Reach goal decoding performance. *A*: average time course of the decoding performance (mean ± SE) using the spike firing rate of 178 neurons in a 200-ms window sliding with 50-ms steps. For each time point, training data and test data were sampled from the 200-ms window ending at that time point. Thick lines represent the accuracy when training and testing data were from the same task. Thin lines represent the accuracy when training and testing data were from different tasks. Dashed horizontal line indicates chance level performance. *B*: same as *A* but using the LFP power of 159 sites. *C*: decoding performance at reach onset as a function of the time window length used to compute the LFP power for both training and testing data. All time windows ended at reach onset. *D*: same as *A* except that the training data for each time point were constant, i.e., the firing rates in the 200 ms ending at reach onset. *E*: same as *D* but using the LFP power. *F*: average LFP power spectra (mean ± SE) across 159 sites for the 200-ms window ending at reach onset vs. the prior 1-s period, from 1,200 ms to 200 ms before reach onset.

without moving their own limbs (Hwang and Andersen 2009). Thus we used data in the 200-ms window ending at reach onset for training the decoders.

The decoding performance increased at a slower rate in this analysis than in the first analysis because of the difference in firing rates between time periods (Fig. 8*D*). However, this is not a concern for prosthetic applications because the performance at reach onset was still perfect in all within- and across-task decoding conditions. Not surprisingly, the decoding performance for one task was not different whether the training data were from the same or the other task because the training data taken at reach onset were almost identical between the two tasks.

The effect of using constant training data on the decoding performance during the early delay period was much stronger when using LFP activity than when using spiking activity (Fig. 8*E*). Using the LFP spectra in the 200-ms window ending at reach onset as training data was bound to produce poor performance in earlier time periods because, in PRR, the LFP spectrum abruptly changes at ~100 ms before reach onset (Hwang and Andersen 2009). More specifically, during the 1-s delay period ending 200 ms before reach onset, oscillation power at 20–40 Hz is stronger than power below 10 Hz in both the direct and symbolic tasks (Fig. 8*F*). However, in the 200-ms window ending at reach onset, the oscillation power at 20–40 Hz is weaker than the power below 10 Hz (Fig. 8*F*). Although the 20–40 Hz power attenuates in the window just before reach onset, the intertask difference in the 20–40 Hz power persists as shown above, decreasing the across-task decoding performance.

Task-invariant goal decoding from PRR spiking activity in other task conditions. We showed that the population spike response allowed task-invariant goal decoding, although 10–30% of the neurons respond differently between the direct and symbolic tasks in terms of their preferred direction, tuning depth, circular variance, and mean firing rate. It is important to know whether task-invariant goal decoding from the population response holds true in other task conditions in which a nonnegligible proportion of neurons have task-specific goal encoding. For instance, we previously showed that ~30% of PRR neurons respond differently when the reach target is visible versus invisible even in the time period near reach onset (Hwang and Andersen 2011). Gail et al. (2009) also showed that their task conditions, i.e., pro- versus antireach, modulated the gain of the response for ~20% of PRR neurons.

To test whether task-invariant decoding occurs in other task conditions, we applied the same decoding analysis to the direct versus visual tasks using the subpopulation of neurons in our present study that were recorded during the visual task in addition to the direct and symbolic tasks ($N = 129$). The visual task was the same as the direct task except that the stimulus at the target location remained illuminated during the delay. As described above, 33% of neurons ($N = 40$) in our present population were visuomotor, showing a higher firing rate in the visual than the direct task prior to reach onset. However, we found that the cross-task decoding performance was as good as the within-task performance, within 100 ms before reach onset (Fig. 9*A*). This indicates that decoding from the spiking activity immediately prior to reach onset is task-invariant even in the presence of a neuronal subpopulation with highly task-specific modulation.

To examine whether the cross-task decoding performance was as good as the within-task performance because a larger proportion of the population ($N = 89$) was not task-specific, we performed neuron dropping curve analysis using all neurons, only the visuomotor neurons, and only the motor neurons, separately (Wessberg et al. 2000). In the neuron dropping curve analysis, decoding was performed on the spiking activity in the 200-ms interval before reach onset. Figure 9*B* shows the cross- and within-task decoding performances in each case. When using visuomotor neurons only the cross-task performance increased with the number of neurons, but it saturated and remained worse than the within-task performance even with as many as 40 neurons. In contrast, when using all neurons or only motor neurons, the cross-task performance became as good as the within-task performance with 40 neurons. The result shows that the task-invariant decoding is achievable if the large proportion of neurons is not task-specific, and can be generalized to various tasks beyond the direct and symbolic tasks.

DISCUSSION

In PRR the spiking activity near reach onset represents the reach goal in a task-invariant manner in the direct and symbolic tasks. The LFP activity in the 20–40 Hz band represents the reach goal more strongly in the symbolic task, but with similar

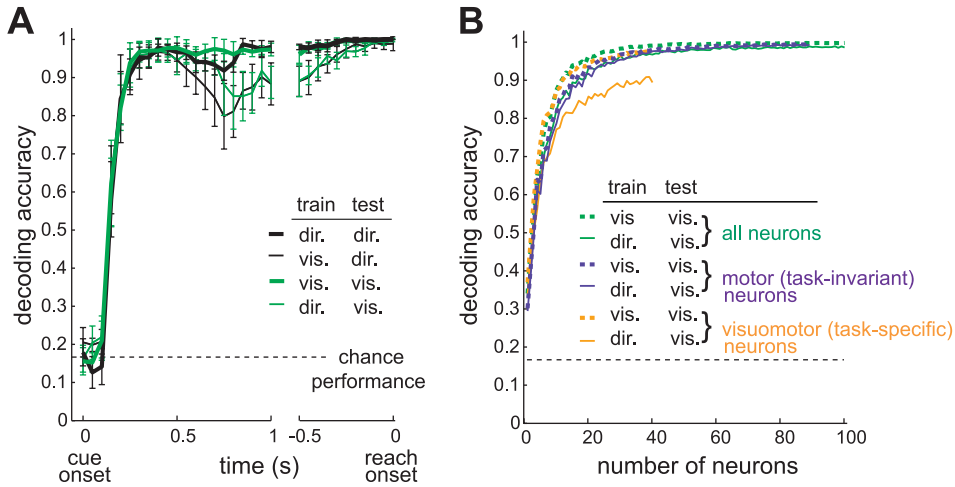

Fig. 9. Task-invariant reach goal decoding at reach onset. *A*: average time course of the decoding performance (mean ± SE) in the direct and visual tasks using the spike firing rate of 129 neurons in a 200-ms window sliding with 50-ms steps. Same format as Fig. 8*A*. *B*: decoding performance at reach onset as a function of the number of neurons used, when using only the visuomotor neurons ($N = 40$), only the motor neurons ($N = 89$), or both ($N = 129$).

spatial preference. The decoder trained with spiking data in one task performed perfectly in the other task even when firing rates were computed over a short time window. In contrast, the decoder trained with LFP data performed significantly worse in the other task than in the same task. These results indicate that a single decoder in PRR, when using the spiking but not LFP activity, can accurately provide the intended goal information in various neural prosthetic applications.

Task-invariant decoding across various task conditions. As mentioned above, the spatial goal of the reach can have various relationships to a visual object (Wise et al. 1996), i.e., direct, transformational, and symbolic. We showed that the task-invariant decoding between direct versus symbolic reaches is possible through the use of the PRR spike population response. The neuron dropping curve analysis indicated that task-invariant decoding is possible if the majority of the neurons are task-invariant (Fig. 9*B*). For instance, despite a significant intertask difference in 33% of the population between the direct and visual tasks, the cross-task decoding performance became as good as 95% correct when using a population of 40 neurons. We did not and cannot test all task conditions possible. However, it has been shown that a majority of PRR neurons encode the reach goal in antireaches similar to proreaches (Gail and Andersen 2006). It was also shown that most PRR neurons encode the reach goal in the presence of two targets similar to a single-target direct task (Scherberger and Andersen 2007). These previous results in combination with the present study results suggest that the intended reach goal can be robustly decoded from PRR spiking activity regardless of the relationship between the visual object(s) and the reach goal.

Implications for neural prosthetic applications. In some neural prosthetic applications (e.g., clicking computer icons and keyboards), decoding the spatial goal of a movement without the detailed kinematics of the movement trajectory is sufficient and even more efficient to operate a prosthetic device than decoding the trajectory (Andersen et al. 2004; Santhanam et al. 2006). Moreover, the intended goal information is also important in applications requiring volitional trajectory control because it can significantly improve the accuracy and speed of prosthetic movements when incorporated into instantaneous kinematic state decoders (Mulliken et al. 2008; Shanechi et al. 2011; Yu et al. 2007). In both types of applications, the goal may be derived directly or symbolically from visual objects. Although it would be possible to build decoders that detect the task condition and use separate decoders depending on the task condition, it will be more convenient and straightforward if neural activity in a region represents the goal information in a task-invariant manner so that the decoder can be trained in a simple calibration task and decode the goal information across various applications. We demonstrated that PRR neurons can serve this purpose.

The task-invariant goal representation held true near reach onset but not earlier (Fig. 3, *A* and *B*, and Fig. 8*A*). However, the variability in the early goal representation is not a concern for prosthetic applications as long as the intended reach onset can be reliably estimated and the decoder uses data selectively in the time window immediately before the intended reach. Importantly, we previously showed that it is possible to decode the intended reach onset from LFPs in PRR based on their abrupt spectrum changes similar to those in Fig. 8*F* (Hwang and Andersen 2009).

Task-variant early period response. At least two factors explain the intertask difference in neural activity in the early period: the stimulus condition and the goal computation time. In sensorimotor areas such as PRR and PMd, among neurons encoding the motor goal, a subpopulation of neurons show a burst of response to visual stimulus onset, possibly encoding the location of the stimulus (Crammond and Kalaska 1994; Gail et al. 2009; Westendorff et al. 2010). In a previous study, we found that ~30% of PRR neurons (visuomotor) and the gamma band LFPs are sensitive to visual stimuli while the other neurons (motor) are not (Hwang and Andersen 2011). The visuomotor neurons and the LFP gamma band power showed higher activity when the reach goal stayed illuminated than when the goal extinguished, although a reach was planned to the same preferred goal in both cases. Not surprisingly, the visuomotor neurons and the gamma band LFPs had strong transient responses upon stimulus onset in their preferred goal location but not the motor neurons.

In the present study, the reach goal was visually cued in the direct task but in the symbolic task the center of the workspace was visually cued. The visual stimulation at the goal location would be expected to elicit more activity for the visuomotor neurons and the gamma band LFPs than the visual stimulation of the central location even though both stimuli instruct a reach to the preferred goal. As expected, we found that the visuomotor neurons and the LFP gamma band power showed significantly stronger early period activity in the direct task compared with the symbolic task (Fig. 3, *A* and *B*, and Fig. 5, *C* and *D*).

Another difference between the two tasks is the complexity of goal computation. It has been shown that more complex tasks are associated with longer reaction times and slower evolution of neural activity encoding the motor response (Gail and Andersen 2006; Roitman and Shadlen 2002). In the direct task, the goal is a direct translation of the stimulus location. In the symbolic task, the identity of the stimulus must first be associated with the correct goal. Thus it is expected that the goal computation would take longer in the symbolic than the direct task. Indeed, we found that both the visuomotor and motor neurons showed later response onset in the symbolic task, reflecting the difference in computation time between the two tasks.

Reach goal tuning of LFPs. Similar to our result, it is commonly found that LFPs encode the same sensory or motor parameters as spikes in the same region but with less sensitivity (Asher et al. 2007; Liu and Newsome 2006; Scherberger et al. 2005). Despite being less sensitive, LFPs are a compelling source of control signals for chronic neural prosthetic applications. Spike recordings become less viable over time, likely in part because of scarring at the electrode tips and movement of the electrodes from cardiac and respiratory pulsations, mechanical movement of the subject, and migration of tissues (Dickey et al. 2009; Santhanam et al. 2007). Because LFPs are less sensitive to changes in the electrode position than spike waveforms (Berens et al. 2008; Frien and Eckhorn 2000; Jia et al. 2011; Leopold and Logothetis 2003; O'Leary and Hatsopoulos 2006; Stark and Abeles 2007), they may be more stable over time than spike signals.

In addition, we found that the reach goal tuning strength of LFPs is not well correlated with the tuning strength of spikes simultaneously recorded from the same recording site. That is, an electrode placed in PRR is likely to record LFP signals carrying goal information whether or not it records spike signals carrying goal information. This result suggests that LFPs can complement spikes to enhance the intended reach goal decoding in neural prosthetic applications. Indeed, this has been confirmed in an actual BMI task in which a monkey controlled a computer cursor position using both spike and LFP signals from 16 electrodes implanted in PRR (Hwang and Andersen 2010). The task performance was significantly better than when either signal was used alone.

At the same time, the present study draws attention to two shortcomings of LFPs for decoding the reach goal. First, for reliable goal estimation, LFP power spectra need to be observed over a longer time window than spike firing rates, limiting their usefulness in tasks requiring fast reactions. Second, LFPs are affected by the task condition more than spikes, and thus more sophisticated decoders must be used when a goal decoder trained with LFPs in one task is used in another task.

The most notable intertask difference was the enhanced reach goal tuning of the 20–40 Hz LFP power in the symbolic task. This is in contrast to the enhanced reach goal tuning of the gamma band power at above 40 Hz in the visual task. However, physiological origins or behavioral correlates of the enhanced LFP power at different frequency bands have yet to be investigated.

ACKNOWLEDGMENTS

We thank Drs. Markus Hauschild, Igor Kagan, Melanie Wilke, Michael Campos, and Bardia Behabadi for scientific discussion, Tessa Yao for editorial assistance, Kelsie Pejsa and Nicole Simmons for animal care, and Viktor Shcherbatyuk for technical assistance.

GRANTS

This work was supported by National Institutes of Health (NIH) Grant EY-013337. E. J. Hwang was supported by NIH Research Service Award T32 NS-007251 and Career Development Award K99 NS-062894.

DISCLOSURES

No conflicts of interest, financial or otherwise, are declared by the author(s).

AUTHOR CONTRIBUTIONS

Author contributions: E.J.H. and R.A.A. conception and design of research; E.J.H. performed experiments; E.J.H. and R.A.A. analyzed data; E.J.H. and R.A.A. interpreted results of experiments; E.J.H. prepared figures; E.J.H. and R.A.A. drafted manuscript; E.J.H. and R.A.A. edited and revised manuscript; E.J.H. and R.A.A. approved final version of manuscript.

REFERENCES

Andersen RA, Cui H. Intention, action planning, and decision making in parietal-frontal circuits. *Neuron* 63: 568–583, 2009.

Andersen RA, Hwang EJ, Mulliken GH. Cognitive neural prosthetics. *Annu Rev Psychol* 61: 169–190, C1–C3, 2010.

Andersen RA, Musallam S, Pesaran B. Selecting the signals for a brain-machine interface. *Curr Opin Neurobiol* 14: 720–726, 2004.

Asher I, Stark E, Abeles M, Prut Y. Comparison of direction and object selectivity of local field potentials and single units in macaque posterior parietal cortex during prehension. *J Neurophysiol* 97: 3684–3695, 2007.

Berens P. *Circular Statistics Toolbox*.

Berens P, Keliris GA, Ecker AS, Logothetis NK, Tolias AS. Comparing the feature selectivity of the gamma-band of the local field potential and the underlying spiking activity in primate visual cortex. *Front Syst Neurosci* 2: 2, 2008.

Churchland MM, Yu BM, Cunningham JP, Sugrue LP, Cohen MR, Corrado GS, Newsome WT, Clark AM, Hosseini P, Scott BB, Bradley DC, Smith MA, Kohn A, Movshon JA, Armstrong KM, Moore T, Chang SW, Snyder LH, Lisberger SG, Priebe NJ, Finn IM, Ferster D, Ryu SI, Santhanam G, Sahani M, Shenoy KV. Stimulus onset quenches neural variability: a widespread cortical phenomenon. *Nat Neurosci* 13: 369–378, 2010.

Crammond DJ, Kalaska JF. Modulation of preparatory neuronal activity in dorsal premotor cortex due to stimulus-response compatibility. *J Neurophysiol* 71: 1281–1284, 1994.

Crammond DJ, Kalaska JF. Prior information in motor and premotor cortex: activity during the delay period and effect on pre-movement activity. *J Neurophysiol* 84: 986–1005, 2000.

Dickey AS, Suminski A, Amit Y, Hatsopoulos NG. Single-unit stability using chronically implanted multielectrode arrays. *J Neurophysiol* 102: 1331–1339, 2009.

Frien A, Eckhorn R. Functional coupling shows stronger stimulus dependency for fast oscillations than for low-frequency components in striate cortex of awake monkey. *Eur J Neurosci* 12: 1466–1478, 2000.

Gail A, Andersen RA. Neural dynamics in monkey parietal reach region reflect context-specific sensorimotor transformations. *J Neurosci* 26: 9376–9384, 2006.

Gail A, Klaes C, Westendorff S. Implementation of spatial transformation rules for goal-directed reaching via gain modulation in monkey parietal and premotor cortex. *J Neurosci* 29: 9490–9499, 2009.

Gur M, Kagan I, Snodderly DM. Orientation and direction selectivity of neurons in V1 of alert monkeys: functional relationships and laminar distributions. *Cereb Cortex* 15: 1207–1221, 2005.

Hwang E, Andersen R. Cognitively driven brain machine control using neural signals in the parietal reach region. In: *Engineering in Medicine and Biology Society (EMBC)*, 2010 Annual International Conference of the IEEE, p. 3329–3332, 2010.

Hwang EJ, Andersen RA. Brain control of movement execution onset using local field potentials in posterior parietal cortex. *J Neurosci* 29: 14363–14370, 2009.

Hwang EJ, Andersen RA. Effects of visual stimulation on LFPs, spikes, and LFP-spike relations in PRR. *J Neurophysiol* 105: 1850–1860, 2011.

Jia X, Smith MA, Kohn A. Stimulus selectivity and spatial coherence of gamma components of the local field potential. *J Neurosci* 31: 9390–9403, 2011.

Leopold DA, Logothetis NK. Spatial patterns of spontaneous local field activity in the monkey visual cortex. *Rev Neurosci* 14: 195–205, 2003.

Liu J, Newsome WT. Local field potential in cortical area MT: stimulus tuning and behavioral correlations. *J Neurosci* 26: 7779–7790, 2006.

Mulliken GH, Musallam S, Andersen RA. Decoding trajectories from posterior parietal cortex ensembles. *J Neurosci* 28: 12913–12926, 2008.

O'Leary JG, Hatsopoulos NG. Early visuomotor representations revealed from evoked local field potentials in motor and premotor cortical areas. *J Neurophysiol* 96: 1492–1506, 2006.

Pesaran B, Pezaris JS, Sahani M, Mitra PP, Andersen RA. Temporal structure in neuronal activity during working memory in macaque parietal cortex. *Nat Neurosci* 5: 805–811, 2002.

Roitman JD, Shadlen MN. Response of neurons in the lateral intraparietal area during a combined visual discrimination reaction time task. *J Neurosci* 22: 9475–9489, 2002.

Salinas E, Abbott LF. Vector reconstruction from firing rates. *J Comput Neurosci* 1: 89–107, 1994.

Santhanam G, Linderman MD, Gilja V, Afshar A, Ryu SI, Meng TH, Shenoy KV. HermesB: a continuous neural recording system for freely behaving primates. *IEEE Trans Biomed Eng* 54: 2037–2050, 2007.

Santhanam G, Ryu SI, Yu BM, Afshar A, Shenoy KV. A high-performance brain computer interface. *Nature* 442: 195–198, 2006.

Scherberger H, Andersen RA. Target selection signals for arm reaching in the posterior parietal cortex. *J Neurosci* 27: 2001–2012, 2007.

Scherberger H, Goodale MA, Andersen RA. Target selection for reaching and saccades share a similar behavioral reference frame in the macaque. *J Neurophysiol* 89: 1456–1466, 2003.

Scherberger H, Jarvis MR, Andersen RA. Cortical local field potential encodes movement intentions in the posterior parietal cortex. *Neuron* 46: 347–354, 2005.

Shanechi M, Williams Z, Wornell G, Brown EN. A brain-machine interface combining target and trajectory information using optimal feedback control. In: *COSYNE*, Salt Lake City, UT, 2011.

Snyder LH, Batista AP, Andersen RA. Coding of intention in the posterior parietal cortex. *Nature* 386: 167–170, 1997.

Stark E, Abeles M. Predicting movement from multiunit activity. *J Neurosci* 27: 8387–8394, 2007.

Stevenson IH, Cherian A, London BM, Sachs NA, Lindberg E, Reimer J, Slutzky MW, Hatsopoulos NG, Miller LE, Kording KP. Statistical assessment of the stability of neural movement representations. *J Neurophysiol* 106: 764–774, 2011.

Thompson KG, Hanes DP, Bichot NP, Schall JD. Perceptual and motor processing stages identified in the activity of macaque frontal eye field neurons during visual search. *J Neurophysiol* 76: 4040–4055, 1996.

Wessberg J, Stambaugh CR, Kralik JD, Beck PD, Laubach M, Chapin JK, Kim J, Biggs SJ, Srinivasan MA, Nicolelis MA. Real-time prediction of hand trajectory by ensembles of cortical neurons in primates. *Nature* 408: 361–365, 2000.

Westendorff S, Klaes C, Gail A. The cortical timeline for deciding on reach motor goals. *J Neurosci* 30: 5426–5436, 2010.

Wise SP, di Pellegrino G, Boussaoud D. The premotor cortex and nonstandard sensorimotor mapping. *Can J Physiol Pharmacol* 74: 469–482, 1996.

Yu BM, Kemere C, Santhanam G, Afshar A, Ryu SI, Meng TH, Sahani M, Shenoy KV. Mixture of trajectory models for neural decoding of goal-directed movements. *J Neurophysiol* 97: 3763–3780, 2007.